Journal of Nuclear Materials 556 (2021) 153176

Contents lists available at ScienceDirect

Journal of Nuclear Materials

journal homepage: www.elsevier.com/locate/jnucmat

Radiation-enhanced diffusion of copper in iron studied by three-dimensional atom probe

T. Toyama[a,*], C. Zhao[a], T. Yoshiie[a,b], S. Yamasaki[c], S. Uno[c], M. Shimodaira[a,#], H. Miyata[a], T. Suzudo[a,d], Y. Shimizu[a,##], K. Yoshida[a], K. Inoue[a], Y. Nagai[a]

[a] Institute for Materials Research, Tohoku University, Oarai, Ibaraki, 311-1313, Japan
[b] Institue for Integrated Radiation and Nuclear Science, Kyoto University, Kumatori, Osaka, 590-0494, Japan
[c] Takasaki Advanced Radiation Research Institute, Quantum and Radiological Science and Technology, Takasaki, Gunma, 370-1292, Japan
[d] Center for Computational Science and e-Systems, Japan Atomic Energy Agency, Tokai, Ibaraki, 319-1195, Japan

ARTICLE INFO

Article history:
Received 11 March 2021
Revised 19 May 2021
Accepted 5 July 2021
Available online 9 July 2021

Keywords:
Radiation effect
Diffusion
Solubility limit
Copper in iron
Atom probe

ABSTRACT

Radiation-enhanced diffusion (RED) of copper (Cu) in iron (Fe) is essential for understanding solute/impurity diffusion in nuclear materials, especially reactor pressure vessel steel, but has been rarely reported experimentally. In this study, we performed a high-precision investigation of RED using well-controlled electron irradiation and three-dimensional atom probe (3D-AP). Cu-Fe diffusion pairs were created using high-purity Fe and Cu as base materials, and irradiated by 2 MeV electron at a temperature of 773 – 893 K controlled to within ±3 K. Cu diffusion into the Fe matrix was observed at the atomic level using 3D-AP, and the diffusion coefficient was obtained directly using Fick's law. RED was clearly observed, and the ratio of diffusion under irradiation to thermal diffusion was increased as the irradiation temperature decreased. RED was quantitatively evaluated using the reaction kinetics model, and the model which consider only vacancies gave a good agreement. This gave experimental clarification that RED was dominated by irradiation-induced vacancies. In addition, the direct experimental results on the effect of irradiation on the solubility limits of Cu in Fe was obtained; solubility limits under irradiation were found to be lower than those under thermal aging.

1. Introduction

Irradiation-induced and/or irradiation-enhanced microstructural changes, such as precipitation and segregation/depletion at the grain boundaries of solute/impurity atoms, are the main origins of nuclear material degradation after irradiation [1,2]. Such microstructural changes are caused by the diffusion of solute/impurity atoms. Because diffusion is dominated by vacancies and/or interstitial atoms, it may be greatly enhanced under irradiation conditions in which large numbers of these defects are introduced, compared with thermal equilibrium conditions. This is known as radiation-enhanced diffusion (RED) [3-10].

The diffusion of copper (Cu) in iron (Fe) is particularly important when considering the irradiation embrittlement of reactor pressure vessel steels (RPVs), as Cu precipitates are the main source of the embrittlement [11-17]. RED for Cu diffusion has been studied theoretically [18-24], however, there is no direct experimental report of RED of Cu in Fe, except for a pioneering study by T. N. Le - (1992) [25], in which the kinetics of Cu precipitation in thermal-aged or electron-irradiated Fe-Cu alloy were examined using electrical resistance measurements and transmission electron microscopy, and the diffusion coefficient (D) of Cu in Fe was determined using a precipitation model. However, it remains challenging to obtain accurate D values from precipitation due to the complex relationship between D and precipitation kinetics. For example, under thermal-aging conditions, D shows a negative dependence on temperature. In addition, the sample temperature, a key parameter in diffusion studies, fluctuated over a broad range of ±15 K during electron irradiation.

To better understand the RED of Cu in Fe, it is necessary to directly evaluate D using Fick's law from the Cu diffusion profiles for Cu-Fe diffusion pairs. Precise control of the sample temperature during irradiation is also essential for RED investigation. In this study, after irradiating the Cu-Fe diffusion pairs with high accu-

* Corresponding author.
# Present: Japan Atomic Energy Agency, Tokai, Ibaraki, 319–1195, Japan
National Institute for Materials Science, Tsukuba, Ibaraki, 305–0047, Japan

https://doi.org/10.1016/j.jnucmat.2021.153176

racy (within ±3 K), the diffusion behavior of Cu was observed using three-dimensional atom probe (3D-AP), allowing direct evaluation of D to reveal the RED of Cu in Fe. We then applied 3D-AP to measure the positions of solute atoms at the atomic level to obtain the Cu concentration profile at very short diffusion lengths (tens of nanometers) for further use in investigating D under thermal-aging conditions [26,27]. Furthermore, we were able to clarify the effect of irradiation on the solubility limit of Cu in Fe, which is another important parameter for the formation of Cu precipitate [18-24] that has not been investigated experimentally to date.

2. Experimental

Pure Fe (5 N, 99.999%) was supplied by Toho Zinc Co. Ltd. (Tokyo, Japan) with hydrogen annealing. The mean residual resistivity ratio was >2000. Pure Cu was supplied by Johnson Matthey (London, UK) at the 5 N grade. Fe was cold-rolled and cut into sheets with dimensions of 10 × 10 × 1 mm^3. After stress-relief annealing and surface cleaning, Fe sheets were coated with a ~5 μm-thick Cu layer using vapor deposition to create Cu-Fe diffusion couples. The average grain size of Fe was 400 – 500 μm. The preparation details are described in our previous study [26].

Electron irradiation for the diffusion couples was performed at the Dynamitron Accelerator of the Quantum and Radiological Science and Technology-Takasaki Advanced Radiation Research Institute. The electron irradiation parameters included an acceleration voltage of 2.0 MeV and total current of 10 mA. The irradiation flux was 3.7 × 10^{13} electron $m^{-2}s^{-1}$, and the rate of the displacement per atom (dpa) was 1.3 × 10^{-9} dpa sec^{-1} assuming the threshold energy of Fe displacement of 40 eV [28]. Only Frenkel pairs were introduced in isolation, which is desirable for studying the basic interactions between irradiation-induced defects and solute atoms. The irradiation conditions was selected to be similar to those of the Le et al. study (2.5 MeV electrons, 2.0 × 10^{-9} dpa sec^{-1}) [25]. The damage rate is also close to that in RPVs (~10^{-10} dpa sec^{-1} [29]).

Irradiation was performed at 773 K for 9 h, 803 K for 9 h, 823 K for 9 h, 843 K for 4 h, and 893 K for 2 h. The sample temperature during electron irradiation was controlled precisely using a custom-designed chamber with thermocouples and electric heaters. Fig. 1 shows the sample temperature during electron irradiation at 893 K as an example of the temperature accuracy obtained, together with the electron beam current. The temperature fluctuation was within ±3 K. During irradiation, helium gas (4 N) flowed into the chamber (volume: ~5 L) at ~0.1 MPa and a rate of ~3 L min^{-1} to prevent sample oxidation.

The needle-shaped specimens for 3D-AP measurements were fabricated using a focused-ion beam apparatus. A piece of the specimen with dimensions of about 5 × 5 × 10 μm^3 was obtained from the intragranular region sufficiently far from the grain boundaries, and then sharpened into a needle form. Finally, very-low energy gallium ions (< 5 kV) were used to remove regions that were potentially damaged during the milling process. The Cu-Fe interface was set near the top of the needle to enable observation of Cu diffusion just below the interface [26].

The 3D-AP measurements were performed using an ultraviolet laser-assisted local-electrode atom probe, LEAP-4000 XHR from AMETEK-CAMECA, to reduce the probability of fracture of specimens, especially around the Cu–Fe interface, at an evaporation rate of 0.6% per a laser pulse, applying a laser power of 50 pJ, a laser pulse repetition rate of 160 kHz, a DC voltage typically in the range of 3 – 8 kV, and specimen temperature of ~35 K. It is known that the estimated Cu concentration in Fe with a laser-assisted atom probe is lower than the best estimate obtained using voltage pulsing atom probe [30]. After preliminary measurements for Fe-0.15 wt.%Cu alloy, the amount of the underestimation in Cu concentration is 10 – 15% in the apparatus in this study, which is similar to the results in Ref. [30].

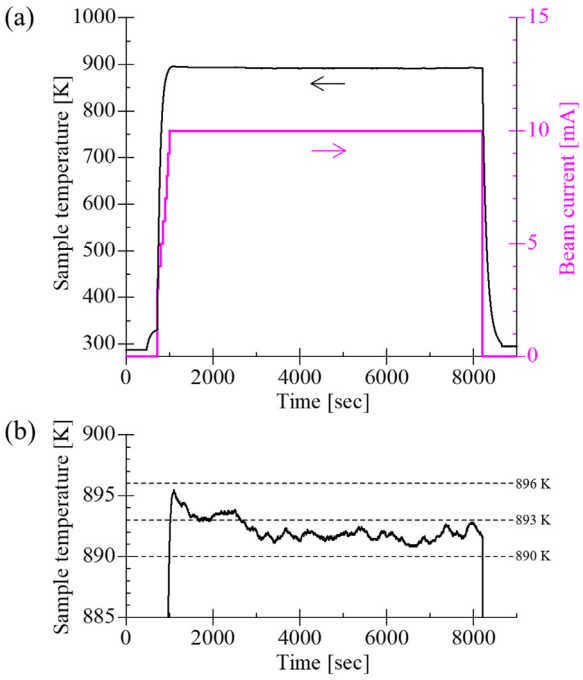

Fig. 1. (a) Time dependency of sample temperature and electron beam current during irradiation at 893 K for 2 h. (b) High-resolution representation of (a). Temperature fluctuation was within ±3 K.

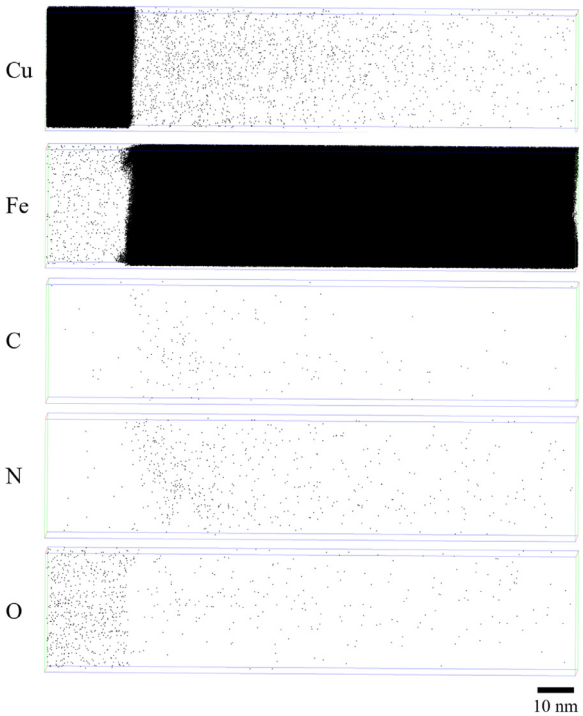

Fig. 2. Typical set of atom maps obtained using 3D-AP for Cu, Fe, C, N, and O for electron-irradiated sample (at 893 K for 2 h).

3. Results

Fig. 2 shows a typical set of atom maps obtained using 3D-AP for Cu, Fe, carbon (C), nitrogen (N), and oxygen (O) for electron-irradiated sample (at 893 K for 2 h). Cu diffusion from the Cu-Fe

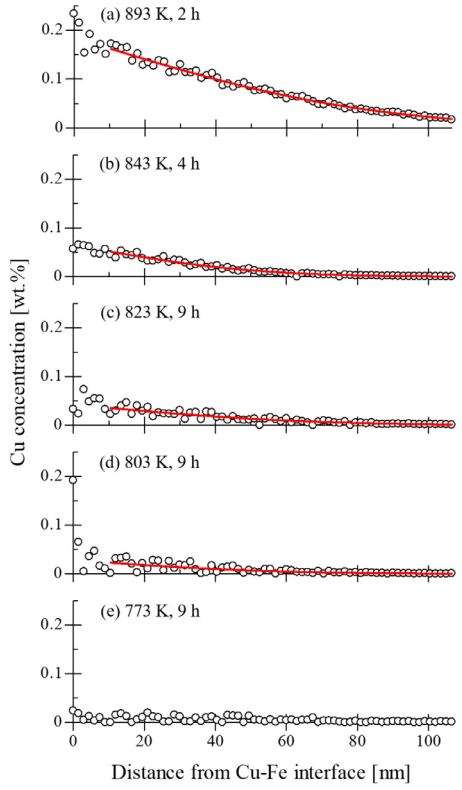

Fig. 3. Cu concentration profiles obtained from a rectangular parallelepiped region (dimensions: 25 × 25 nm^2) in a cross-section perpendicular to the Cu-Fe interface for electron-irradiated samples; (a) at 893 K for 2 h, (b) at 843 K for 4 h, (c) at 823 K for 9 h, (d) at 803 K for 9 h, and (e) at 773 K for 9 h. Fitting curves by Eq. (1) are also shown by red solid curves.

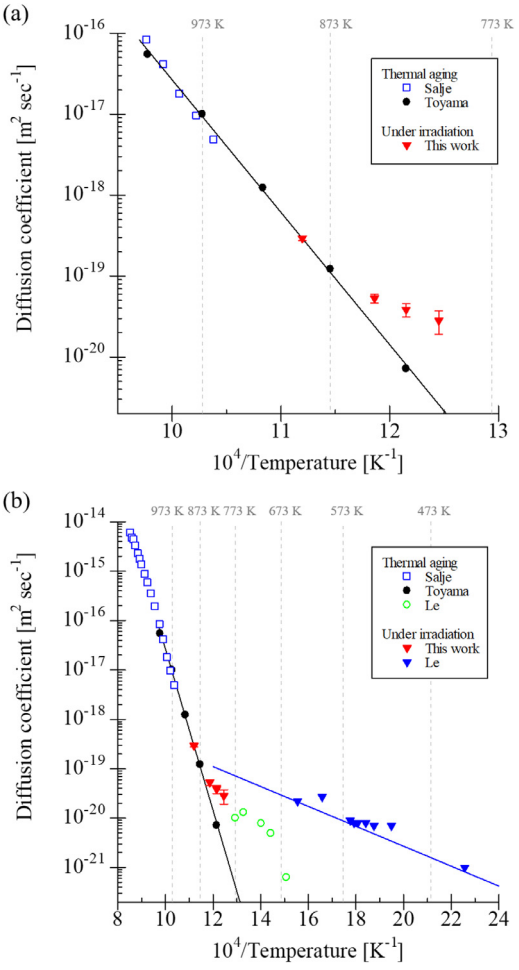

Fig. 4. (a) Arrhenius plots of D under thermal-aged ($D^{thermal}$) [26,32] and D under electron-irradiated (D^{irrad}). The black line is the trend line for $D^{thermal} = 0.48\exp(-3.22/k_BT)$ [26]. (b) Arrhenius plots of $D^{thermal}$ and D^{irrad}, compared with the results in Ref. [25]. The blue lines the trend line for $D^{irrad} = 2.9 \times 10^{-17}\exp(-0.4/k_BT)$ [25].

interface towards the Fe matrix was observed. Impurities, such as C, N, and O, were seldom observed in the Fe matrix; the measured amounts of the impurities were ~8 atppm C, ~15 atppm N, and ~20 atppm O. These values were consistent with our previous results [26]. No segregation of impurities was observed near the Cu-Fe interface, and no Cu clustering in Fe matrix was detected with the statistics analysis.

Fig. 3 shows the Cu concentration profiles obtained from a rectangular parallelepiped region (dimensions: 25 × 25 nm^2) in a cross-section perpendicular to the Cu-Fe interface. Cu diffusion towards the Fe matrix was clearly observed, with the exception of the case at 773 K for 9 h due to the low solubility of Cu in Fe at this low temperature.

Assuming a concentration-independent D, a semi-infinite medium, and a constant surface concentration, Fick's second law gives

$$c(x,t) = c_0 \times erfc(x/(2\sqrt{Dt})) \quad (1)$$

where $c(x, t)$ is the concentration profile, x is the distance from the interface, t is the diffusion time, c_0 is the constant saturation concentration of Cu in Fe according to the diffusion temperature (i.e., the solubility limit of Cu), $erfc$ is a complementary error function, and D is the diffusion coefficient [31]. The measured profiles were fitted to Eq. (1), using c_0 and D as the fit parameters. The fitting results are indicated by red solid curves in Fig. 3. For the sample irradiated at 773 K, fitting was not performed because the observed Cu concentration was < 0.05 wt.%, which is close to the background level.

The diffusion coefficients of Cu in Fe for the irradiated samples, D^{irrad}, were (2.9 ± 0.2) × 10^{-19} m^2 s^{-1} for 893 K, (5.3 ± 0.7) × 10^{-20} m^2 s^{-1} for 843 K, (3.9 ± 0.7) × 10^{-20} m^2 s^{-1} for 823 K, and (2.8 ± 0.9) × 10^{-20} m^2 s^{-1} for 803 K. Arrhenius plots of D^{irrad} are shown in Fig. 4(a), together with the reported values for the non-irradiated (thermal-aged) condition, $D^{thermal}$ [26,32]. D^{irrad} for 893 K is on the trend line of $D^{thermal}$; thus, almost no irradiation effect was observed. However, D^{irrad} for temperatures below 843 K were higher than the trend line. The enhancement factor defined by $D^{irrad}/D^{thermal}$ was 0.91 for 893 K, 2.0 for 843 K, 4.2 for 823 K, and 9.5 for 803 K. The enhancement factor increased as the irradiation temperature decreased, indicating an increase in the effect of irradiation at lower temperatures. Fig. 4(b) shows Arrhenius plots of D^{irrad} and $D^{thermal}$ together with the results of Le et al. [25]. Although the irradiation conditions of the present study were similar to those of the Le et al. study, the D^{irrad} values obtained in the two studies are very different.

In Eq. (1), c_0 is equivalent to the solubility limit of Cu in Fe. The obtained solubility limits for the irradiated samples, c_0^{irrad}, were (0.19 ± 0.01) wt.% for 893 K, (0.065 ± 0.01) wt.% for 843 K, (0.042 ± 0.01) wt.% for 823 K, and (0.028 ± 0.02) wt.% for 803 K. The correlation between temperature and c_0^{irrad} is shown in Fig. 5. The reported values for the non-irradiated (thermal-aged) condition, $c_0^{thermal}$, are also shown [26,32,33]. For the present and our previous data [26], there could be underestimations in Cu concentration due to a laser-assisted 3D-AP, 15% in maximum. The corrected values, divide of the original values by 0.85, are also shown

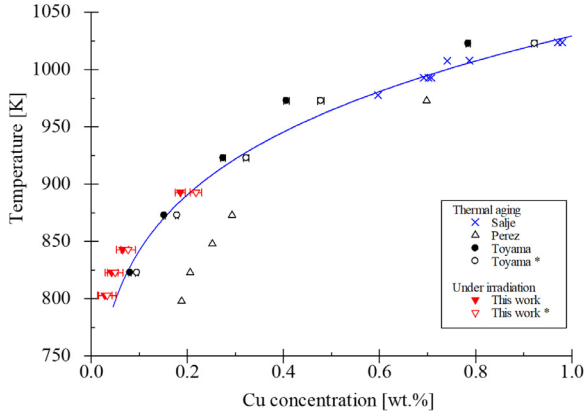

Fig. 5. Solubility limit of Cu in Fe under thermal-aged ($c_0 th^{ermal}$) [26,32,33] and under electron-irradiated ($c_0{}^{irrad}$). The trend curve is log $c_0 th^{ermal} = 4.495–4627/T$ [32]. For the data marked with * in the legend, the detection efficiency of Cu in a laser-assisted 3D-AP measurement is corrected (see the text).

Table 1
Physical parameters used in this study.

Parameter	Value
P	1.3×10^{-9} s $^{-1}$
Z_{IV}	100 [34,36]
$E_V{}^m$	0.70 eV [37]
$E_I{}^m$	0.33 eV [38]
N	1 × 1013 s $^{-1}$ [34]
C_S	1×10^{-9}, 1×10^{-7}, 1×10^{-5}

marked with * in the legend. The obtained values of $c_0{}^{irrad}$ were somewhat lower than those of $c_0{}^{thermal}$.

4. Discussion

We quantitatively evaluated the observed RED of Cu in Fe using the reaction kinetics model. In the first step, the vacancy (interstitial) concentration induced by irradiation, $C_V{}^{irrad}$ ($C_I{}^{irrad}$), is estimated. According to the model,

$$dC_V^{irrad}/dt = P - K_{IV}C_I^{irrad}C_V^{irrad} - K_{VS}C_V^{irrad}C_S$$
$$dC_I^{irrad}/dt = P - K_{IV}C_I^{irrad}C_V^{irrad} - K_{IS}C_I^{irrad}C_S$$

where P is the production rate of vacancy or interstitial, K_{IV} is the rate of vacancy-interstitial recombination, and K_{VS} (K_{IS}) is the annihilation rate of vacancy (interstitial) to the sink, and C_S is the concentration of sink for vacancy or interstitial [3]. The formation of di-vacancy (di-interstitial) or larger vacancy (interstitial) clusters is neglected. K_{IV}, K_{VS}, and K_{IS} are set at $K_{IV} = Z_{IV}(\exp(-E_V{}^m/k_BT) + \exp(-E_I{}^m/k_BT))$, $K_{VS} = \nu\exp(-E_V{}^m/k_BT)$, and $K_{IS} = \nu\exp(-E_I{}^m/k_BT)$, respectively, where Z_{IV} is the site number of spontaneous recombination, $E_V{}^m$ ($E_I{}^m$) is the migration energy of vacancy (interstitial), ν is the vibration frequency, and k_B is the Boltzmann constant [34,35]. In the present study, the candidate of the dominant sinks are the surface and the Cu-Fe interface, because the specimens for 3D-AP measurement were fabricated from the region near the surface/interface but far from grain boundaries. If the surface is the dominant sink, the expected jump times for vacancy (interstitial) from the region near the Cu-Fe interface to the sink will be ~$(2 \times 10^4)^2$, because the necessary migration length is ~5 μm which corresponds to ~2×10^4 atomic distance. Assuming that C_S as the inverse of the jump times, C_S is ~3×10^{-9}. In case of the Cu-Fe interface, C_S is ~6×10^{-6} with the migration length of ~100 nm. Therefore, we set the values of C_S as 1×10^{-9}, 1×10^{-7}, and 1×10^{-5}. The physical parameters used in this study are listed in Table 1.

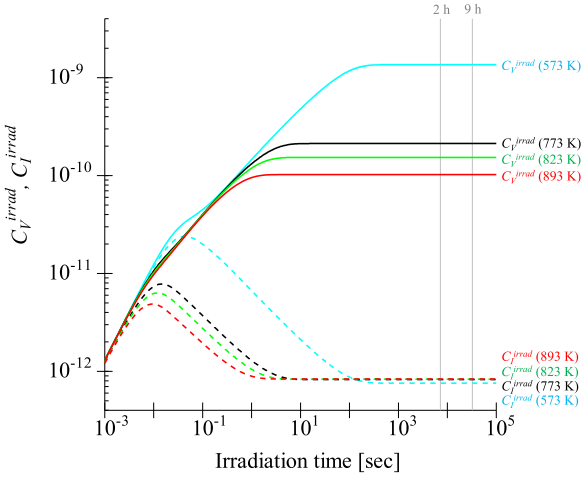

Fig. 6. Irradiation time dependency of $C_V{}^{irrad}$ and $C_I{}^{irrad}$ calculated using the reaction kinetics model ($C_S = 1 \times 10^{-9}$).

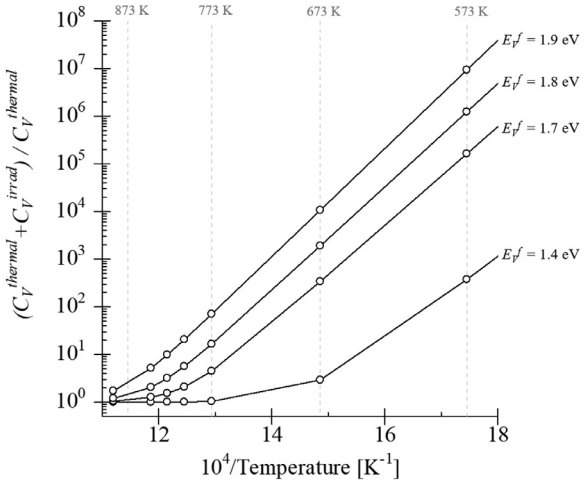

Fig. 7. Irradiation temperature dependency of $(C_V{}^{thermal} + C_V{}^{irrad}) / C_V{}^{thermal}$ ($C_S = 1 \times 10^{-9}$).

Fig. 6 shows the irradiation time dependency of $C_V{}^{irrad}$ and $C_I{}^{irrad}$ calculated using the reaction kinetics model with $C_S = 1 \times 10^{-9}$. We obtained a similar trend to those reported in previous studies [3,7,39]. For each irradiation temperature, $C_V{}^{irrad}$ reaches a constant value after several seconds. In case of $C_S = 1 \times 10^{-7}$ and 1×10^{-5}, the time $C_V{}^{irrad}$ reaches a constant value is shorter than in $C_S = 1 \times 10^{-9}$. Therefore, the phenomena observed in the present study occurred during the steady state.

Fig. 7 shows the irradiation temperature dependency of $(C_V{}^{thermal}+C_V{}^{irrad})/C_V{}^{thermal}$ with $C_S = 1 \times 10^{-9}$ where $C_V{}^{thermal}$ is the vacancy concentration at thermal equilibrium condition. The value of $C_V{}^{irrad}$ was set to be the value at the end of each irradiation period shown in Fig. 6, and the value of $C_V{}^{thermal}$ was evaluated as follows:

$$C_V^{thermal} = exp\left(S^f/k_B\right) \times exp\left(-E_V^f/k_BT\right)$$

where S^f is the entropy and $E_V{}^f$ is the vacancy formation energy. S^f/k_B was set at 2, and $E_V{}^f$ was set to range from 1.4 [40] to 2.0 eV [41]. As shown in Fig. 7, $(C_V{}^{thermal}+C_V{}^{irrad})/C_V{}^{thermal}$ increased as temperature decreased.

In the second step, D^{irrad} is estimated. $D^{thermal}$ and D^{irrad} are expressed as follows:

$$D^{thermal} = D_V C_V^{thermal} + D_I C_I^{thermal} \sim D_V C_V^{thermal}$$
$$D^{irrad} = \left(C_V^{thermal} + C_V^{irrad}\right)D_V + \left(C_I^{thermal} + C_I^{irrad}\right)D_I \quad (2)$$

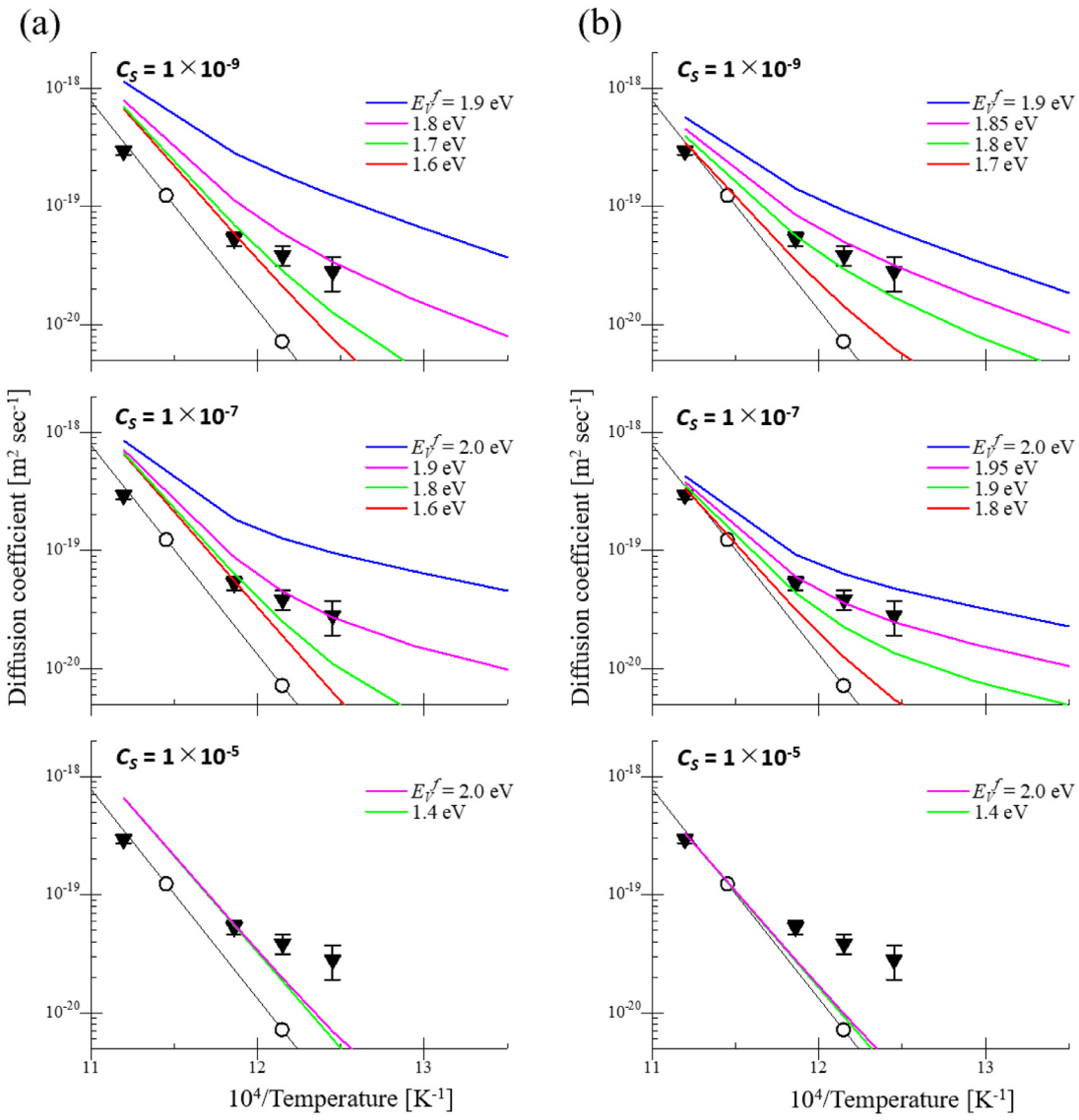

Fig. 8. Arrhenius plots of D^{irrad} evaluated using the reaction kinetics model with several values of C_S and E_V^f. D^{irrad} in this work (black close triangles) and $D^{thermal}$ in Ref. [26] (black open circles) are also shown; (a) D^{irrad} is evaluated by Eq. (3). (b) D^{irrad} is evaluated by Eq. (4).

where D_V (D_I) corresponds to the diffusion by vacancy (interstitial) mechanism and $C_I^{thermal}$ is the interstitial concentration at thermal equilibrium condition [3,42]. For self-diffusion at steady state, it is known that vacancies and interstitials contribute equally to atom mobility, namely, $(C_I^{thermal}+C_I^{irrad})D_I \sim (C_V^{thermal}+C_V^{irrad})D_V$ [1,3]. Then, Eq. (2) is modified as

$$D^{irrad} = \left(C_V^{thermal} + C_V^{irrad}\right)D_V + \left(C_I^{thermal} + C_I^{irrad}\right)D_I \sim 2\left(C_V^{thermal} + C_V^{irrad}\right)D_V$$

Therefore,

$$D^{irrad}/D^{thermal} = 2\left(C_V^{thermal} + C_V^{irrad}\right)/C_V^{thermal} \quad (3)$$

On the other hand, if the contribution of interstitials to the diffusion is negligible, Eq. (2) is modified as

$$D^{irrad} = \left(C_V^{thermal} + C_V^{irrad}\right)D_V + \left(C_I^{thermal} + C_I^{irrad}\right)D_I \sim \left(C_V^{thermal} + C_V^{irrad}\right)D_V$$

Therefore,

$$D^{irrad}/D^{thermal} = \left(C_V^{thermal} + C_V^{irrad}\right)/C_V^{thermal} \quad (4)$$

D^{irrad} was evaluated by Eq. (3) or Eq. (4) with $(C_V^{thermal}+C_V^{irrad})/C_V^{thermal}$ shown in Fig. 7 and $D^{thermal} = 0.48\exp(-3.22/k_BT)$ [26], as shown in Figs. 8(a) and (b), together with the experimental values of D^{irrad} obtained in this study. D^{irrad} evaluated by Eq. (4) shown in Fig. 8(b) agreed better with the experimental values. The best fit was given by Eq. (4) with $C_S = 1 \times 10^{-7}$ and $E_V^f = 1.95$ eV.

The fact that Eq.4 rather than Eq. (3) gave a good fitting indicates that the contribution of interstitials to the diffusion is negligibly small. This agrees well with the prediction by theoretical studies that the contribution of interstitials is negligible for Cu in Fe matrix even under irradiation [38,43], because oversized Cu solutes in Fe matrix have repulsive interaction with interstitials thus the mixed dumbbells are rarely formed [37]. Therefore, we conclude that the RED of Cu in Fe observed in this study was caused by the irradiation-induced vacancies.

The D^{irrad} values obtained in this study are significantly different from those obtained by Le et al. [25], who determined the D from Cu precipitation kinetics, measured the residual Cu concentration in the Fe matrix and number density of Cu precipitates experimentally, and then applied a precipitation model to estimate D. The precipitation model assumes uniformity of precipitate size, constant number density of precipitates during precipitation, and

that only Cu diffusion dominates precipitate growth. The resulting model is an oversimplification of the precipitation process, and therefore estimates D with considerable inaccuracy, as noted in the original publication (as we reported [44], it is possible to obtain D more accurately using precipitation kinetics by considering the attractive interaction between Cu atoms). In addition to these problem with the precipitation model, the accuracy of the experimental values in Ref. [25] was insufficient due to difficulties in quantitative evaluation of the deviation from Matthiessen's rule for electrical resistance measurements [1].

Although recent developments in computer simulation have allowed theoretical investigation of RED for Cu and other elements, such as chromium and nickel, after [18-24,45-49], very few studies have examined RED for Cu in Fe experimentally. We anticipate that the results of the present study, which were obtained by applying Fick's second law directly to the Cu diffusion profiles of Cu-Fe diffusion pairs, will come to represent a benchmark with respect to the validation of theoretical studies by allowing direct comparison of experimental and theoretical studies.

It is suggested that the effect of irradiation on solubility limit strongly depends on irradiation conditions (damage rate and temperature), because it is dominated by the effect of irradiation on the second phase formation [9,50]. When the second phase formation is promoted due to RED and/or an increase of the formation sites for example, the solubility limit decreases. As an example, significant decrease of zinc (Zn) solubility in aluminum (Al) matrix was observed in dilute Al-Zn alloys under very high damage rates of 10^{-2} and 10^{-4} dpa sec^{-1}, which is due to radiation-induced precipitation of Zn [51]. In this study, a slight decrease of the solubility limit of Cu in Fe was observed. While irradiation conditions and materials are incomparable, this is the same trend as reported in Ref. [51]. However, it would not be explained by the promotion of the second phase formation because no Cu clustering was detected in this study. The possible origin may be solid solution destabilization under irradiation [50], while it is still open question. Further exploration for the effect of irradiation on solubility limit of Cu in Fe is necessary, and experimentally in progress by using dilute Fe-Cu alloys.

5. Conclusion

Radiation-enhanced diffusion (RED) of Cu in Fe was investigated with high precision using well-controlled electron irradiation and 3D-AP. Cu-Fe diffusion pairs were created from high-purity Fe and Cu as base materials, and irradiated by 2 MeV electron at a temperature of 773 – 893 K controlled to within ±3 K. Cu diffusion into the Fe matrix was observed using 3D-AP, and D^{irrad} was obtained through direct application of Fick's law. RED was clearly observed, and the enhancement factor, $D^{irrad}/D^{thermal}$, was increased as the irradiation temperature decreased. Quantitative evaluation of RED using a reaction kinetics model revealed that the model which consider only vacancies gave a good agreement, indicating that RED was dominated by irradiation-induced vacancies. In addition, the direct experimental results on the effect of irradiation on the solubility limit of Cu in Fe was obtained; solubility limits under irradiation were found to be lower than those under thermal aging.

Declaration of Competing interest

The authors declare that they have no known competing financial interests or personal relationships that could have appeared to influence the work reported in this paper.

CRediT authorship contribution statement

T. Toyama: Conceptualization, Investigation, Formal analysis, Writing – original draft. **C. Zhao:** Investigation. **T. Yoshiie:** Writing – review & editing. **S. Yamasaki:** Investigation. **S. Uno:** Investigation. **M. Shimodaira:** Investigation. **H. Miyata:** Investigation. **T. Suzudo:** Formal analysis. **Y. Shimizu:** Formal analysis. **K. Yoshida:** Formal analysis. **K. Inoue:** Formal analysis. **Y. Nagai:** Supervision.

Acknowledgement

The authors are grateful for insights provided by Professor S. Nishitani at Kwansei Gakuin Univ., Professor T. Ichitsubo at Tohoku Univ., and Dr. K. Ebihara at JAEA. The authors thank the helpful supports from N. Ebisawa, Y. Nozawa, K. Tomura, H. Hanaya, and K. Daikubara. This work was partly support by JSPS KAKENHI Grant Numbers 26709073, 17H03517, and 20H02661. This work was performed under The Inter-University Program for the Joint-Use of JAEA/QST Facilities, the Univ. of Tokyo (17007, 18007, and 19008), and the GIMRT Program of IMR, Tohoku Univ. (18M0405, 19M0407, and 20M0406).

Reference

[1] G.S. Was, Fundamentals of Radiation Materials Science, Springer, 2007.
[2] K.L. Murty, Materials' Ageing and Degradation in Light Water Reactors, Woodhead Publishing Limited, 2013.
[3] R. Sizmann, The effect of radiation upon diffusion in metals, J. Nucl. Mater. 69&70 (1968) 386–412.
[4] A. Seeger, The mechanisms of diffusion in metals and alloys, J. Less Common Metals 28 (2) (1972) 387–418.
[5] N.Q. Lam, S.J. Rothman, Radiation-enhanced Diffusion in Metals and Alloys, Argonne National Laboratory, 1975.
[6] M. Kiritani, Electron radiation induced diffusion of point defects in metals, J. Phys. Soc. Jpn. 40 (4) (1976).
[7] C. Abromeit, R. Poerschke, Radiation enhanced diffusion: approximate solutions of chemical rate equations and their application to experiments, J. Nucl. Mater. 82 (1979) 298–301.
[8] S.J. Rothman, Phase Transformations During Irradiation, Applied Science Publishers Ltd, 1983.
[9] G. Martin, Phase stability under irradiatoin: ballistic effects, Phys. Rev. B 30 (1984) 1424.
[10] K.C. Russell, Phase stability under irradiation, Prog. Mater. Sci. 28 (1984) 229–434.
[11] G.R. Odette, G.E. Lucas, Irradiation embrittlement of reactor pressure vessel steels: mechanisms, Models, and Data Correlations, ASTM STP 909 (1986) 206–241.
[12] G.R. Odette, G.E. Lucas, Embrittlement of Nuclear Reactor Pressure Vessels, JOM 53 (7) (2001) 18–22.
[13] T. Toyama, Y. Nagai, Z. Tang, M. Hasegawa, A. Almazouzi, E. van Walle, R. Gerard, Nanostructural evolution in surveillance test specimens of a commercial nuclear reactor pressure vessel studied by three-dimensional atom probe and positron annihilation, Acta Mater. 55 (20) (2007) 6852–6860.
[14] G.R. Odette, R.K. Nanstad, Predictive reactor pressure vessel steel irradiation embrittlement models: issues and opportunities, Jom 61 (7) (2009) 17–23.
[15] K. Fukuya, Current understanding of radiation-induced degradation in light water reactor structural materials, J. Nucl. Sci. Technol. 50 (3) (2013) 213–254.
[16] G.R. Odette, Recent Progress in Developing and Qualifying Nanostructured Ferritic Alloys for Advanced Fission and Fusion Applications, Jom 66 (12) (2014) 2427–2441.
[17] G.R. Odette, T. Yamamoto, T.J. Williams, R.K. Nanstad, C.A. English, On the histroy and status of reactor pressure vessel steel ductile to brittle transition temperature shift predictioni models, J. Nucl. Mater. 526 (2019) 151863.
[18] F. Soisson, G. Martin, A. Barbu, Copper precipitation in dilute iron-copper alloys: a Monte Carlo simulation, Ann. Phys. (Paris) 20 (3) (1995) 13–20.
[19] F. Soisson, A. Barbu, G. Martin, Monte Carlo simulations of copper precipitation in dilute iron-copper alloys during thermal ageing and under electron irradiation, Acta Mater. 44 (9) (1996) 3789–3800.
[20] M. Athenes, F. Soisson, P. Bellon, G. Martin, Solid State Diffusion and Configurational Kinetics, The Japan Institute of Metals, 1999.
[21] F. Soisson, C.-.C. Fu, Cu-precipitation kinetics in a-Fe from atomistic simulations: vacancy-trapping effects and Cu-cluster mobility, Phys. Rev. B 76 (21) (2007) 214102.
[22] L. Malerba, G.J. Ackland, C.S. Becquart, G. Bonny, C. Domain, S.L. Dudarev, C.C. Fu, D. Hepburn, M.C. Marinica, P. Olsson, R.C. Pasianot, J.M. Raulot, F. Soisson, D. Terentyev, E. Vincent, F. Willaime, Ab initio calculations and interatomic potentials for iron and iron alloys: achievements within the Perfect Project, J. Nucl. Mater. 406 (2010) 7–18.

[23] F. Soisson, C.S. Becquart, N. Castin, C. Domain, L. Malerba, E. Vincent, Atomistic Kinetic Monte Carlo studies of microchemical evolutions driven by diffusion processes under irradiation, J. Nucl. Mater. 406 (2010) 55–67.
[24] V.G. Vaks, F. Soisson, I.A. Zhuravlev, Studies of homogeneous precipitation in very dilute iron-copper alloys using kinetic Monte Carlo simulations and statistical theory of nucleation, Philos. Mag. 93 (23) (2013) 3084–3109.
[25] T.N. Le, A. Barbu, D. Liu, F. Maury, Precipitation kinetics of dilute FeCu and FeCuMn alloys subjected to electron irradiation, Scr. Metall. Mater. 26 (1992) 771–776.
[26] T. Toyama, F. Takahama, A. Kuramoto, H. Takamizawa, Y. Nozawa, N. Ebisawa, M. Shimodaira, Y. Shimizu, K. Inoue, Y. Nagai, The diffusivity and solubility of copper in ferromagnetic iron at lower temperatures studied by atom probe tomography, Scr. Mater. 83 (2014) 5–8.
[27] M. Shimodaira, T. Toyama, F. Takahama, N. Ebisawa, Y. Nozawa, Y. Shimizu, K. Inoue, Y. Nagai, Diffusivity and Solubility of Cu in a Reactor Pressure Vessel Steel Studied by Atom Probe Tomography, Mater. Trans. 56 (9) (2015) 1513–1516.
[28] O.S. Oen, Cross Sections For Atomic Displacements in Solids By Fast Electrons, Oak Ridge National Lab, 1973.
[29] G.R. Odette, B.D. Wirth, A computational microscopy study of nanostructural evolution in irradiated pressure vessel steels, J. Nucl. Mater. 251 (1997) 157–171.
[30] J.M. Hyde, M.G. Burke, B. Gault, D.W. Saxey, P. Styman, K.B. Wilford, T.J. Williams, Atom probe tomography of reactor pressure vessel steels: an analysis of data integrity, UltramicroscopyUltramicroscopy 111 (6) (2011) 676–682.
[31] P. Shewmon, Diffuion in Solids, Springer International Publishing, 2016.
[32] G. Salje, M. Feller-Kniepmeier, The diffusion and solubility of copper in iron, J. Appl. Phys. 48 (1977) 1833.
[33] M. Perez, F. Perrard, V. Massardier, X. Kleber, A. Deschamps, H.D. Monestrol, P. Pareige, G. Covarel, Low-temperature solubility of copper in iron: experimental study using thermoelectric power, small angle X-ray scattering and tomographic atom probe, Philos. Mag. 85 (2005) 2197–2210.
[34] S. Yanagita, T. Yoshiie, H. Ino, A model calculation for irradiation rate dependence of defect structure in Fe-Cu alloy, J. Jpn. Inst. Met. 64 (2) (2000) 115–124.
[35] T. Yoshiie, Q. Xu, K. Sato, K. Kikuchi, M. Kawai, Reaction kinetics analysis of damage evolution in accelerator driven system beam windows, J. Nucl. Mater. 377 (2008) 132–135.
[36] N. Yoshida, M. Kiritani, F.E. Fujita, ELECTRON RADIATION-DAMAGE OF IRON IN HIGH-VOLTAGE ELECTRON-MICROSCOPE, J. Phys. Soc. Jpn. 39 (1) (1975) 170–179.
[37] L. Messina, M. Nastar, T. Garnier, C. Domain, P. Olsson, Exact ab initio transport coefficients in bcc Fe-X (X=Cr, Cu, Mn, Ni, P, Si) dilute alloys, Phys. Rev. B 90 (10) (2014).
[38] L. Messina, T. Schuler, M. Nastar, M.-.C. Marinica, P. Olsson, Solute diffusion by self-interstitial defects and radiation-induced segregation in ferritic Fe–X (X=Cr, Cu, Mn, Ni, P, Si) dilute alloys, Acta Mater. 191 (2020) 166–185.
[39] K.P. Gurov, A.B. Tsepelev, The kinetics of radiation point defect accumulation in metals during irradiation, J. Nucl. Mater. 182 (1991) 240–246.
[40] S.M. Kim, W.J.L. Buyers, Vacancy formation energy in iron by positron annihilation, J. Phys. F: Metal Phys. 8 (1978) L103.
[41] L. De Schepper, D. Segers, L. Dorikens-Vanpraet, M. Dorikens, G. Knuyt, L.M. Stals, P. Moser, Positron annihilation on pure and carbon-doped a-iron in thermal equilibrium, Phys. Rev. B 27 (1983) 5257.
[42] H. Wiedersich, CHAPTER 4 - Phase Stability and Solute Segregation during Irradiation* *Work supported by the U.S. Department of Energy, in: R.A. Johnson, A.N. Orlov (Eds.), Modern Problems in Condensed Matter Sciences, Elsevier, 1986, pp. 225–280.
[43] L. Huang, M. Nastar, T. Schuler, L. Messina, Multiscale modeling of the effects of temperature, radiation flux, and sink strength on point-defect and solute redistribution in dilute Fe-based alloys, Phys. Rev. Mater. 5 (3) (2021) 033605.
[44] C. Zhao, T. Suzudo, T. Toyama, S. Nishitani, K. Inoue, Y. Nagai, Investigation of Cu Diffusivity in Fe by a Combination of Atom Probe Experiments and Kinetic Monte Carlo Simulation, Materials Transactions 62 (7) (2021) 929–934.
[45] N. Castin, M.I. Pascuet, L. Malerba, Mobility and stability of large vacancy and vacancy-copper clusters in iron: an atomistic kinetic Monte Carlo study, J. Nucl. Mater. 429 (1–3) (2012) 315–324.
[46] G. Stechauner, E. Kozeschnik, Thermo-kinetic modeling of Cu precipitation in alpha-Fe, Acta Mater. 100 (2015) 135–146.
[47] S.P. Shu, P. Bellon, R.S. Averback, Role of point-defect sinks on irradiation-induced compositional patterning in model binary alloys, Phys. Rev. B 91 (21) (2015) 13.
[48] F. Soisson, T. Jourdan, Radiation-accelerated precipitation in Fe-Cr alloys, Acta Mater. 103 (2016) 870–881.
[49] N. Castin, G. Bonny, C. Domain, J.M. Hyde, L. Messina, B. Radiguet, L. Malerba, The dominant mechanisms for the formation of solute-rich clusters in low-Cu steels under irradiation, Mater. Today Energy 17 (2020) 100472.
[50] R. Cauvin, G. Martin, Solid-solutions under irradiation .1. a model for radiation-induced metastability, Phys. Rev. B 23 (7) (1981) 3322–3332.
[51] R. Cauvin, G. Martin, Solid-solutions under irradiation .2. radiation-induced precipitation in alzn undersaturated solid-solutions, Phys. Rev. B 23 (7) (1981) 3333–3348.